AIP | Applied Physics Letters

High transition temperature superconductor/insulator bilayers for the development of ultra-fast electronics

M. Sirena, L. Avilés Félix, and N. Haberkorn

Citation: Applied Physics Letters **103**, 052902 (2013); doi: 10.1063/1.4816416
View online: http://dx.doi.org/10.1063/1.4816416
View Table of Contents: http://scitation.aip.org/content/aip/journal/apl/103/5?ver=pdfcov
Published by the AIP Publishing

High transition temperature superconductor/insulator bilayers for the development of ultra-fast electronics

M. Sirena,[1,2] L. Avilés Félix,[1,2] and N. Haberkorn[1]
[1]*Consejo Nacional de Investigaciones Científicas y Técnicas, Centro Atómico Bariloche, CNEA, Bustillo 9500, 8400 Bariloche, Argentina*
[2]*Instituto Balseiro, Universidad Nacional de Cuyo & CNEA, 8400 Bariloche, Argentina*

(Received 26 April 2013; accepted 25 June 2013; published online 29 July 2013)

High transition temperature superconductor (HTc)/$SrTiO_3$ (STO) bilayers were fabricated by sputtering deposition on (100) STO substrates. Their transport and morphological properties were characterized using conductive atomic force microscopy. The STO barriers present good insulating properties, with long attenuation lengths ($\lambda \sim 1$ nm) which reduce the junction resistance and increase the operating critical current. The samples present roughness values smaller than 1 nm, with an extremely low density of surface defects ($\sim 5 \times 10^{-5}$ defects/μm^2). The high control of the barrier quality over large defect free surfaces is encouraging for the development of microelectronics devices based in HTc Josephson junctions. © *2013 AIP Publishing LLC*.
[http://dx.doi.org/10.1063/1.4816416]

Tunnel junctions (TJ) like devices typically consist of two conducting electrodes separated by a thin insulating barrier, in which the current flows in the direction perpendicular to the surface. TJ present a wide range of applications, going from spintronics (magnetic tunnel junctions,[1] spin filters,[2] etc.) to superconducting electronics using Josephson junctions (JJ)[3] or even molecular junctions.[4] Transport properties of superconducting JJ are governed by the tunnelling of the fundamental particles (cooper pairs) across the barrier due to the proximity effect. The transport properties of the system depend on the phase coherence between the superconductor electrodes and give place to a great number of technological applications, such as superconducting quantum interference devices (SQUID) for measuring extremely low magnetic signals, or complex integrated JJ arrays for ultra fast electronics, using rapid single flux quantum logic.[5] In JJ, one of the key parameters for their performance is the junction energy which is related directly with the superconducting gap as discussed in the paper of Josephson. The higher the energy of the junction compared with the thermal energy is the larger the signal to noise ratio.[6] Moreover, high junction energies allow higher operation frequencies. Indeed, the importance of high transition temperature superconducting (HTc) electrodes is not related to higher operating temperatures but to much higher superconducting gaps than those present in low transition temperature superconductors, as indicated by Anders *et al*.

The insulating barrier is a fundamental component in TJ like devices. The thickness and homogeneity of the barrier must assure a good covering of the electrodes while being thin enough to provide a good coupling between them (i.e., low resistance for magnetic tunnel junctions or high critical current for JJ). Moreover, insulating barriers of different nature (e.g., ferromagnetic, ferroelectric, etc.) can be used to develop different functionalities, like spin filtering barriers, showed in the paper of Foerster *et al*. or the electric control of the tunnelling current.[7] In order to optimize the fabrication process and to characterize the properties of different barrier types, good knowledge and control of the barrier properties at the nanoscale are critical.

In the last years, there has been an increasing interest in combining ferroelectric compounds with superconducting materials. The origin of this interest is the possibility to control the superconducting properties with the application of an external electrical field. Taking advantage of this, the ferroelectric polarization can affect the transport properties of thin superconducting films in a non-volatile way. The origin of this interest is related not only with aspects of basic physics but also with several technological challenges (e.g., the developing of electrical field transistors, on-off resistance switching devices, superconducting memristors, etc.). Several research groups have attempted to fabricate HTc superconducting JJ (typically using $YBa_2Cu_3O_7$ (YBCO) electrodes) with $SrTiO_3$ (STO) barriers due to the good structural compatibility. Moreover, recent results seem to show that highly strained STO thin films could present ferroelectricity at room temperature,[8–10] making stressed STO layers, suitable barriers for the development of superconducting/ferroelectric heterostructures. However, the growth of high quality STO barriers over YBCO electrodes has been difficult. YBCO electrodes present a high density of surface defects reducing the homogeneity and the energy barrier value for YBCO/STO bilayers, especially for the relative large dimensions required for the fabrication of some devices. The scope of this work is to optimize and characterize the fabrication of HTc superconductor/STO bilayers for the fabrication of JJ. The fabrication of high quality stressed STO barriers would be the first step for the development of superconductor based devices with different functionalities.

We have recently developed a phenomenological approach and a characterization analysis using conductive atomic force microscopy to study the transport and morphological properties of thin insulting layers over conducting electrodes.[11] We have applied this method to study the growth of thin STO barriers over $GdBa_2Cu_3O_{7-\delta}$ (GBCO) thin electrodes.

Thin GBCO and STO bilayers were grown on SrTiO3 (100) crystalline substrates by DC and low power (25 W) RF magnetron sputtering, respectively. The substrate temperature was kept at 795 °C in an argon (90%)/oxygen (10%)

atmosphere at a pressure of 400 mTorr. After deposition, the temperature was decreased to 500 °C, and the O_2 pressure was increased to 100 Torr. Finally, the samples were cooled down to room temperature at a rate of 1.5 °C/min. We have used thin GBCO electrodes (15 ± 1 nm) in order to reduce the roughness of the surface, increasing the quality of the STO barrier as deduced from the work of M. Sirena. STO layers of different thicknesses (d: 1 nm, 1.5, 2.5, and 3.5 nm) were deposited over the HTc superconducting electrode. A GBCO (15 nm)/STO (3.5 nm) bilayer, with a post deposition annealing in a reduced oxygen pressure (5 Torr), was fabricated in order to test the influence of oxygen vacancies in the physical properties of the system. The superconducting transition temperature (Tc) of the electrodes, obtained from transport measurements, is 75 K.[12] A reduction of the Tc is expected probably due to an oxygen content in the samples different from the optimum value.

CAFM measurements were performed in a Dimension 3100 © Bruker microscope, using diamond doped conductive tips at room temperature. A complete characterization of the samples was made by analyzing the topographic and CAFM current information at different scale lengths (2.5 μm, 15 μm, and 124 μm). In order to increase reproducibility, the images were taken using the same deflection point (i.e., the same tip-surface pressure) and the same polarization voltage (2 V).[13] To avoid any surface charge or chemical alteration of the surface due to tip-sample interaction, all the images were taken in "virgin," previously untouched areas. Samples were measured within two or three days from the deposition date in order to reduce any possible passivation of the surface (significant changes in the transport properties were not observed until the samples were exposed for several days in air). Current-voltage (I(V)) responses of the samples were measured at different surface spots (typically around 10) in order to reduce dispersion and electrical noise. To assure the perfect condition of the tip, high resolution images of the samples were taken and compared to previous measured data, checking the sharpness of the images and the absence of any experimental artefacts.

Figure 1 presents the I(V) curves of GBCO/STO bilayers for different insulating thicknesses ($d = 0$ nm (HTc electrode), 1 nm, 1.5 nm, 2.5 nm, and 3.5 nm). The GBCO electrode presents a non-linear behavior of the current voltage characteristics; this is usually the case for oxide electrodes due to the passivation of the surface exposed to the air. The measured current for the electrodes presents a smaller variation with the applied voltage than the observed for the bilayers. Current–voltage values give an idea of the electrode's conductance, which can be compared with the conductance of the pinholes, observed in CAFM images. The bilayers present a power law dependence of the current as function of the applied voltage. This is coherent with the tunnelling of the transport carriers across an insulating barrier. The fit of the experimental data shows a linear dependence of the fitting parameters with the barrier thickness. It can be shown that this dependence leads to $I(V,d) = I_0 V^{\alpha_0} e^{-\frac{d}{\lambda}}$, where λ is the attenuation length of the charge carriers in the barrier.[14] Short attenuation lengths indicate an extremely fast decay of the tunnelling current, corresponding to high insulating barriers. In the traditional Simmons's model, for the high

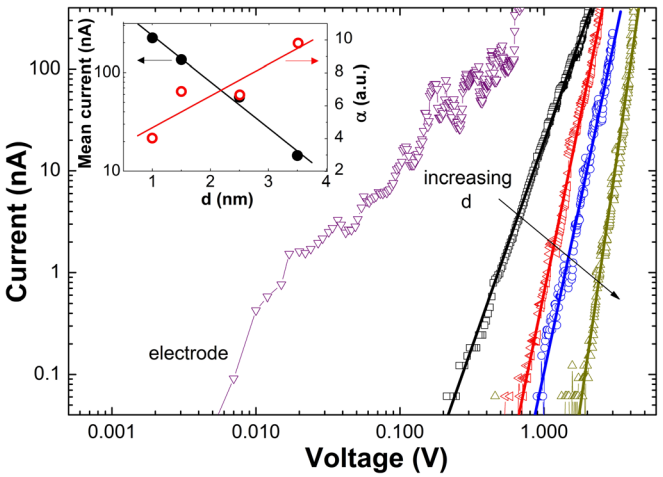

FIG. 1. I(V) curves for the GBCO/STO bilayers with different thicknesses of the STO barrier ($d = 0$ nm (electrode only), 1 nm, 1.5 nm, 2.5 nm, and 3.5 nm). The solid lines are linear fits of the experimental data ($Log(I) = A_0(d) + \alpha(d) \cdot Log(V)$). The inset presents the average values of α as a function of d, obtained from the fitting of the I(V) curves and the mean current as function of d, obtained from the CAFM images.

voltage regime ($V > \phi$, where ϕ is the energy barrier), the same dependence for the tunnelling current can be found, with $\alpha_0 = 2$. For GBCO/STO bilayers, α_0 is around 2.7. Recently, we have found that in real systems with insulating layers grown over different electrodes (YBCO, Nb, or ferromagnetic oxides such as $La_{0.75}Sr_{0.25}MnO_3$) the tunnelling current presents a more abrupt dependence with the applied voltage. Moreover, the more insulating the barrier (λ smaller) is the higher α_0 seems to be.[15] This is coherent with our results. The reduction of the tunnelling current with increasing barrier thickness for GBCO/STO bilayers is smaller than the observed for YBCO/STO bilayers, and in the latter, α_0 is around 3.5, larger than the value obtained for this system (~2.7). The quadratic dependence of the tunnelling current with the polarization voltage is related with a rectangular barrier shape and more fundamentally to a linear change of the energy barrier with the applied voltage, indicating that in these systems a more important change of the barrier with the polarization voltage is expected.

The 2.5 μm × 2.5 μm topographical and CAFM current images of different samples are shown in Figure 2. The CAFM image of the electrode was acquired using a lower polarization voltage due to its higher conductivity. The stability of the CAFM current image of the GBCO film was lower than for the bilayers, probably due to some passivation of the sample surface. The topographical information indicates that the samples present a surface of good quality with 1 nm (~1 unit cell) terraces (see the topographical section analysis in Fig. 3) and very low root mean square roughness between 0.5 nm and 1 nm; similar values were obtained for 15 μm × 15 μm images. The good surface quality of the samples could be related with the low thickness of the electrodes, the deposition technique, or a good chemical stability of the GBCO electrode. CAFM images show that as the thickness of the barrier increases the tunnelling current decreases. However, the decrease of the current is lower than the one observed in similar systems by Félix and coworkers, e.g., YBCO/STO bilayers grown by pulsed laser deposition. The mean current as a function of the barrier thickness

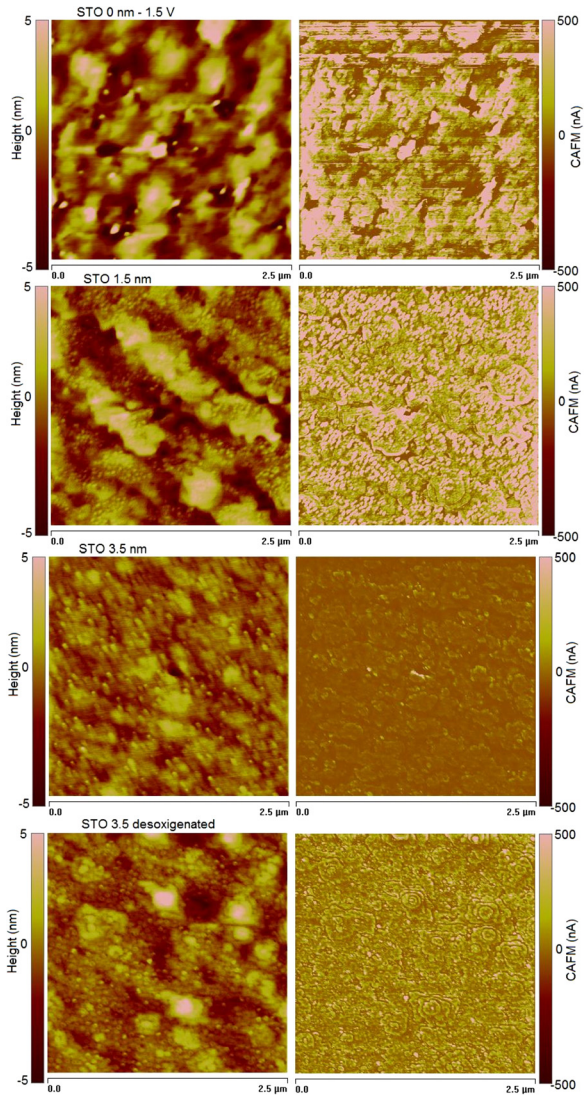

FIG. 2. Topographic (left) and CAFM (right), 2.5 μm × 2.5 μm, images of GBCO/STO bilayers with different STO thicknesses. The applied voltage was 2 V. The bottom panel corresponds to a 3.5 nm layer annealed in a reduced oxygen atmosphere.

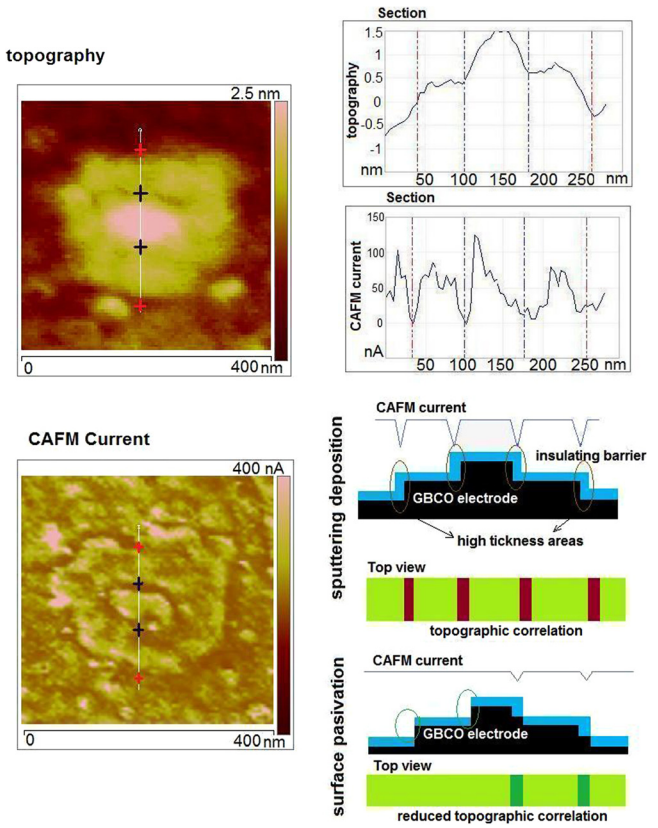

FIG. 3. Topographic and CAFM current analysis of a surface defect (shown for the GBCO/STO (3.5 nm) bilayer with a post deposition annealing in a reduced oxygen pressure). Schematic view of the CAFM current, transversal image of the bilayers, and the CAFM images resulting from the sputtering deposition of the insulating layer and the oxide formation in the sample due to the passivation of the surface.

is shown in the inset of Figure 1. Even though the mean current values are higher than expected, the current decays exponentially as the insulator layer thickness increases, indicating that tunnelling is probably the main transport mechanism in these samples. The attenuation length, obtained by the linear fit of the experimental data, is around 1 nm, three times larger than the attenuation length obtained for YBCO/STO bilayers. Higher attenuation lengths can be induced by morphological disorder as it was shown in the work of Sirena. However, this is probably not the case for our samples due to the high quality of their surface and the low roughness. Another possibility is a poor oxygenation of the STO layer. It is known that oxygen deficient STO films present a higher conductivity and even a metal-insulator transition for increasing oxygen vacancies.[16] The topographic and CAFM current images of a GBCO/STO bilayer, with a post deposition oxygen annealing in a reduced oxygen pressure, are shown in the bottom panel of Figure 2. The sample presents the morphological quality of the oxygenated samples, but the corresponding CAFM current is higher. I(V) curves of the sample show a non linear behavior. It should be noticed that the annealing in a reduced oxygen atmosphere could also affect the oxygen content in the HTc electrode. This could affect the superconducting properties of the electrode, i.e., its transition temperature and its critical current density (Jc) affecting the transport trough the barrier at low temperatures. Moreover, changing the oxygen content in the GBCO electrode should change its lattice parameter affecting the lattice mismatch with the STO layer.[17] Preliminary results of CAFM measurements in $La_{0.7}Sr_{0.3}MnO_3$/STO and GBCO/STO bilayers, grown under different oxygenation processes, indicate that the strain field in the barrier could affect the transport properties of the system. A more complete report about the oxygen and strain effects in the tunnelling properties of STO barriers will be presented shortly.

Interestingly, the correlation between CAFM current images and the topography of the sample could give important information about the growth mechanism of the insulating layer and the covering of the conducting electrode. Figure 3 shows the topographical and CAFM current images and section analysis of a typical surface defect (shown for the bilayer with oxygen deficiency). It is possible to see that when the CAFM tip goes over the terrace walls the tunnelling current decreases. The width and the triangular shape of the current drop is probably related to the tip resolution (∼20 nm), indicating that the terraces present abrupt walls. Assuming that the tunnelling current fluctuations can be ascribed to thickness variations of the barrier, the drop of the

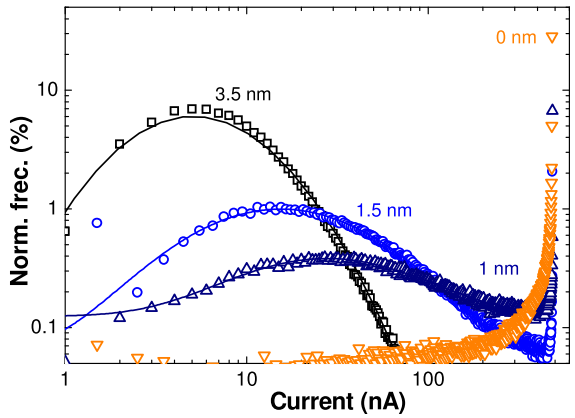

FIG. 4. Current distributions for GBCO/STO bilayers. The data correspond to different thicknesses of the barrier ($\nabla = 0$ nm, $\Delta = 1$ nm, $O = 1.5$ nm, and $\square = 3.5$ nm) at 2 V. The lines are the fittings using a log-normal distribution.

current could indicate that the effective barrier thickness in the terrace walls is higher (e.g., the distance between the CAFM tip and the closer conducting surface, given by the border of the terrace, is larger than the barrier thickness). A schematic view of the barrier deposition by physical methods (e.g., sputtering, pulsed laser deposition, etc.) can be seen in Figure 3. To simplify the discussion the schematic view corresponds to the case in which the barrier thickness is smaller than the height of the steps. However, it is possible to see that considering a barrier thickness larger than the step height leads to the same results. The growth mechanism induces an important topographical correlation of the CAFM current. On the other hand an oxide layer could be formed by the passivation or oxidation of the surface. In this case the oxide layer is formed in the surface of the electrode (there is no actual deposition but a modification of the surface). Assuming that the insulated layer is formed only in the surfaces with high contact area with the oxidation atmosphere (and no diffusion), the passivation occurs manly in the areas parallel to the sample surface (i.e., in the terraces steps and not in the terraces walls), and no topographical correlation can be seen in the CAFM images (Figure 3). This is probably the case for important areas of the GBCO electrode.

As mentioned before, the tunnelling current dispersion in CAFM measurements can be generally ascribed to a barrier thickness distribution. Assuming a Gaussian distribution for the insulating layer thickness, the exponential dependence of the tunnelling current with the barrier thickness gives place to a lognormal current distribution.[18] Figure 4 shows the CAFM current distributions for the GBCO/STO bilayers with different insulating layer thicknesses. The lognormal distribution seems to fit well the experimental data. As the thickness of the barrier increases the current distribution shifts to lower values, as expected. The CAFM current dispersion corresponds to a thickness distribution width of 0.8 nm, in good agreement with the measured roughness values. The critical thickness to totally cover the electrodes is around 3 nm. This seems a little high taking into consideration the low roughness of the samples, but it could be related with the type the morphology of the defects. Surface defects in the samples present important height gradients and abrupt walls that easily break the insulating layer. On the other hand, the large attenuation length would reduce the resistance of the JJ based in GBCO/STO bilayers, even for "thick" barriers, increasing the critical current for applications. Large critical currents are desirable to facilitate detection and to reduce the electrical noise. Additionally, thick ($d > 3$ nm) barriers are in general necessary in order to assure ferroelectricity.[19]

Finally, Figure 5 presents a high scale (124 μm $\times$ 124 μm) topography and CAFM current images of a 3.5 nm GBCO/STO bilayer with an applied polarization voltage of 3 V. A high polarization voltage was used in order to stress the measurement conditions and the barrier homogeneity. Large up and down stripes in the background of the topographic images are experimental artefacts due to the piezoelectric movement for large scan sizes. It was rather difficult to obtain a perfect stable CAFM image for this large scan size, probably due to the long scan times. In order to have the same tip velocity, the scan speed was reduced in a factor of 10–0.1 Hz. It is noteworthy the important reduction of the surface defects density ($\sim 5 \times 10^{-5}$ def/μm^2), compared with similar systems, made by other techniques. This is probably related with the sputtering technique used for the fabrication of the samples, in which we used a low RF power deposition of the STO barrier and also a better chemical stability of the GBCO electrode.

Reproducibility is a critical issue for the development of ultra fast microelectronics devices using Josephson junctions. Further studies are needed to correctly evaluate the

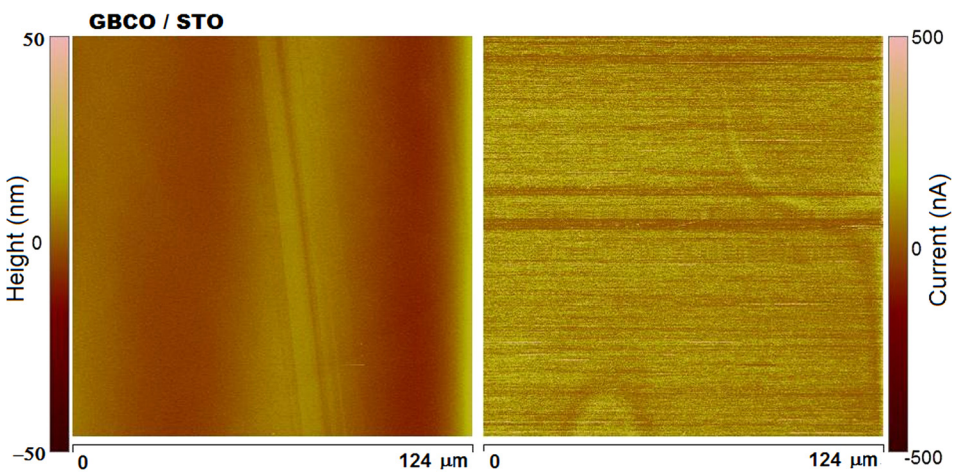

FIG. 5. Topographic (left) and CAFM (right) 124 μm $\times$ 124 μm images of a GBCO/STO bilayer with a STO thickness of 3.5 nm. The polarization voltage was 3 V.

reproducibility in these systems. However, our results show a nice control of the barrier properties, over HTc superconducting electrodes of high morphological quality. The STO barrier presents good insulating properties, with larger attenuation lengths, allowing to reduce the junction resistance and increasing the operating critical current of the Josephson junctions. The samples present low roughness with an extremely low density of surface defects. These are encouraging results for the development of HTc JJ based ultra-fast microelectronics and the search of different functionalities in superconducting devices.

The authors would like to thank R. Benavides for his extraordinary technical support. The authors would also like to recognize the important work, help, and support from Dr. J. Guimpel and Dr. H. Pastoriza for the use of the micro and nanofabrication facilities and A. Butera for the critical reading of the manuscript. This work was partially supported by the ANPCYT (PICT PRH 2008-109) and Universidad Nacional de Cuyo (06/C395).

[1]J. S. Moodera, L. R. Kinder, T. M. Wong, and R. Meservey, Phys. Rev. Lett. **74**, 3273 (1995).
[2]M. Foerster, F. Rigato, K. Bouzehouane, and J. Fontcuberta, J. Phys. D **43**, 295001 (2010).
[3]B. D. Josephson, Phys. Lett. **1**, 251 (1962).
[4]A. C. Kummel, Science **302**, 69 (2003).
[5]S. Anders, M. G. Blamire, F.-I. Buchholz, D.-G. Crété, R. Cristiano, P. Febvre, L. Fritzsch, A. Herr, E. Il'ichev, J. Kohlmann *et al.*, Physica C **470**, 2079 (2010).
[6]N. Bergeal, J. Lesueur, M. Sirena, G. Faini, M. Aprili, J. P. Contour, and B. Leridon, J. Appl. Phys. **102**, 083903 (2007).
[7]A. Crassous, R. Bernard, S. Fusil, K. Bouzehouane, J. Briatico, M. Bibes, A. Barthélémy, and J. E. Villegas, J. Appl. Phys. **113**, 024910 (2013).
[8]J. H. Haeni, P. Irvin, W. Chang, R. Uecker, P. Reiche, Y. L. Li1, S. Choudhury, W. Tian, M. E. Hawley, B. Craigo, A. K. Tagantsev, X. Q. Pan, S. K. Streiffer, L. Q. Chen, S. W. Kirchoefer, J. Levy, and D. G. Schlom, Nature (London) **430**, 758 (2004).
[9]H. W. Jang, A. Kumar, S. Denev, M. D. Biegalski, P. Maksymovych, C. W. Bark, C. T. Nelson, C. M. Folkman, S. H. Baek, N. Balke, C. M. Brooks, D. A. Tenne, D. G. Schlom, L. Q. Chen, X. Q. Pan, S. V. Kalinin, V. Gopalan, and C. B. Eom, Phys. Rev. Lett. **104**, 197601 (2010).
[10]W. J. Maeng, I. Jung, and J. Y. Son, Solid State Commun. **152**, 1256 (2012).
[11]M. Sirena, J. Appl. Phys. **110**, 063923 (2011).
[12]N. Haberkorn, G. Bridoux, E. Osquiguil, G. Nieva, and J. Guimpel, Appl. Surf. Sci. **254**, 222 (2007).
[13]K. M. Lang, D. A. Hite, R. W. Simmonds, R. McDermott, P. Pappas, and J. M. Martinis, Rev. Sci. Instrum. **75**, 2726 (2004).
[14]J. G. Simmons, J. Appl. Phys. **34**, 1793 (1963).
[15]L. A. Félix, M. Sirena, L. A. A. Guzmán, J. G. Sutter, S. P. Vargas, L. B. Steren, R. Bernard, J. Trastoy, J. E. Villegas, J. Briático, N. Bergeal, J. Lesueur, and G. Faini, Nanotechnology **23**, 495715 (2012).
[16]I. Pallecchi, G. Grassano, D. Marre, L. Pellegrino, M. Putti, and A. S. Siri, Appl. Phys. Lett. **78**, 2244 (2001); P. Calvani, M. Capizzi, F. Donato, S. Lupi, P. Maselli, and D. Peschiaroli, Phys. Rev. B **47**, 8917 (1993).
[17]J. M. S. Skakle, Mater. Sci. Eng. R. **23**, 1 (1998).
[18]F. Bardou, Europhys. Lett. **39**, 239 (1997); V. Da Costa, M. Romeo, and F. Bardou, J. Magn. Magn. Mater. **258–259**, 90 (2003).
[19]G. Gerra, A. K. Tagantsev, N. Setter, and K. Parlinski, Phys. Rev. Lett. **96**, 107603 (2006).